Chapter 7,8,9

waveguides

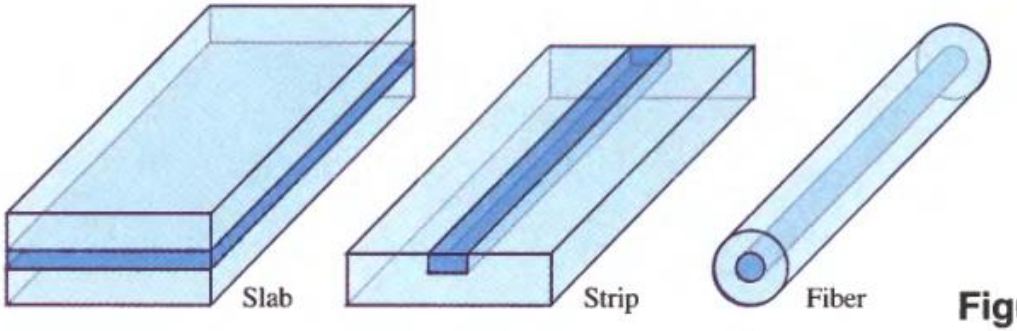

Figure 8.0-1 Optical waveguides.

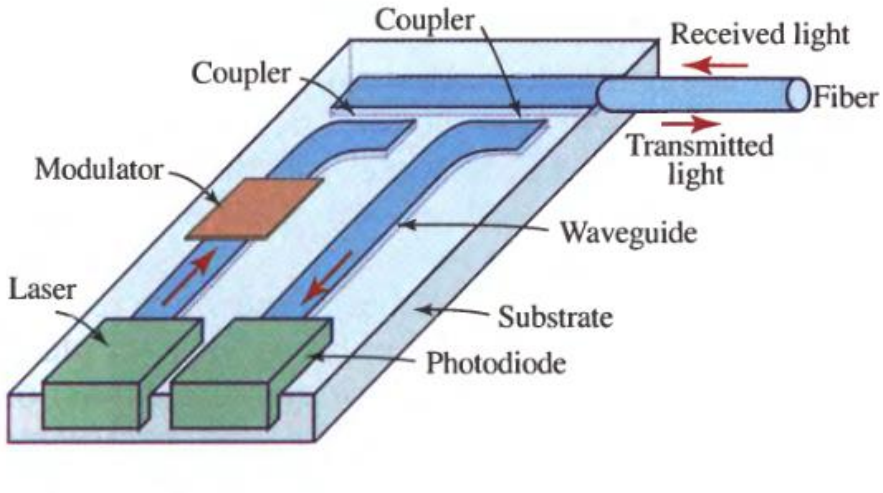

Figure 8.0-2 Example of an integrated-optic device used as an optical receiver/transmitter. Received light is coupled into a waveguide and directed to a photodiode where it is detected. Light from a laser is guided, modulated, and coupled into a fiber for transmission.

Planar mirror waveguide

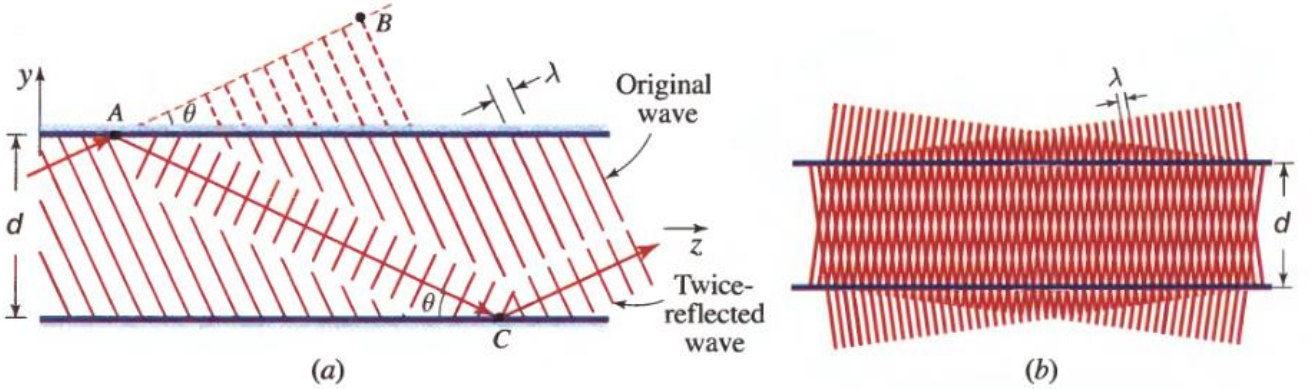

Figure 8.1-2 (*a*) Condition of self-consistency: as a wave reflects twice it duplicates itself. (*b*) At angles for which self-consistency is satisfied, the two waves interfere and create a pattern that does not change with z.

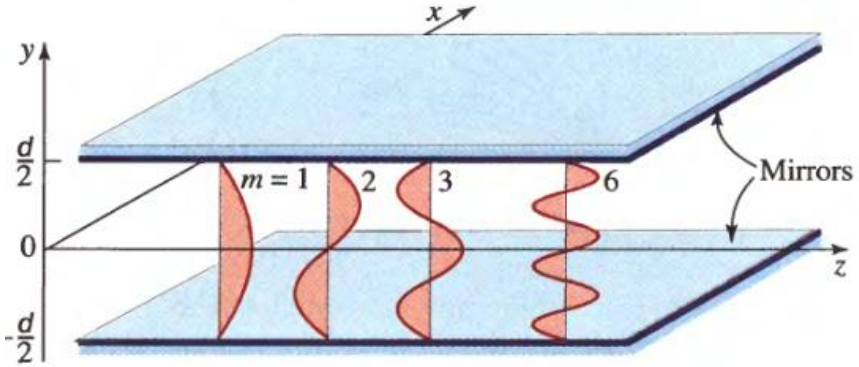

Figure 8.1-4 Field distributions of the modes of a planar-mirror waveguide.

Planar mirror waveguide

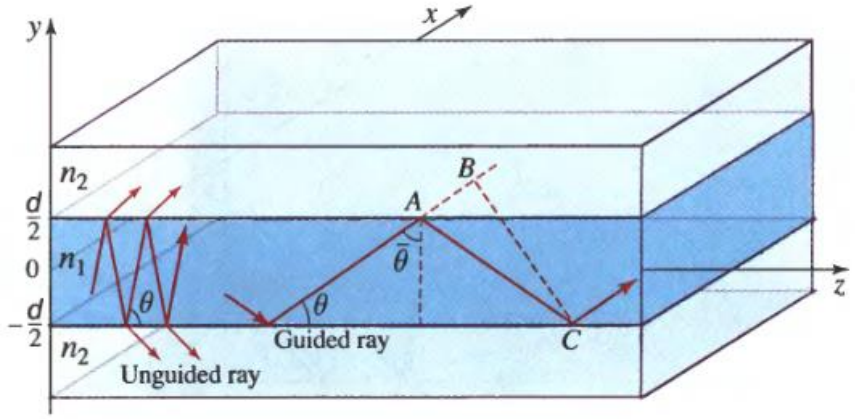

Figure 8.2-1 Planar dielectric (slab) waveguide. Rays making an angle $\theta < \theta_c = \cos^{-1}(n_2/n_1)$ are guided by total internal reflection.

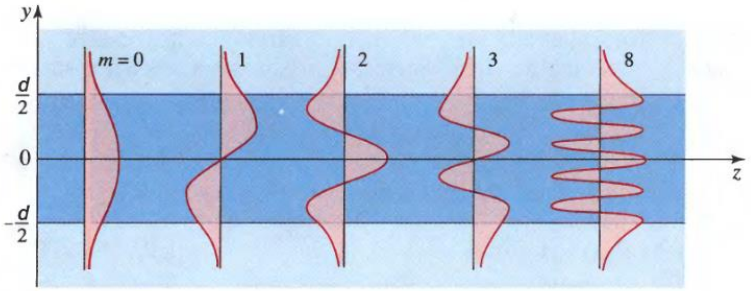

Figure 8.2-5 Field distributions for TE guided modes in a dielectric waveguide. These results should be compared with those shown in Fig. 8.1-4 for the planar-mirror waveguide.

$$u_m(y) \propto \begin{cases} \cos\left(2\pi \dfrac{\sin\theta_m}{\lambda} y\right), & m = 0, 2, 4, \ldots \\ \sin\left(2\pi \dfrac{\sin\theta_m}{\lambda} y\right), & m = 1, 3, 5, \ldots, \end{cases} \qquad -\frac{d}{2} \le y \le \frac{d}{2}, \quad (8.2\text{-}10)$$

$$u_m(y) \propto \begin{cases} \exp(-\gamma_m y), & y > d/2 \\ \exp(\gamma_m y), & y < -d/2. \end{cases}$$

Various waveguide geometries

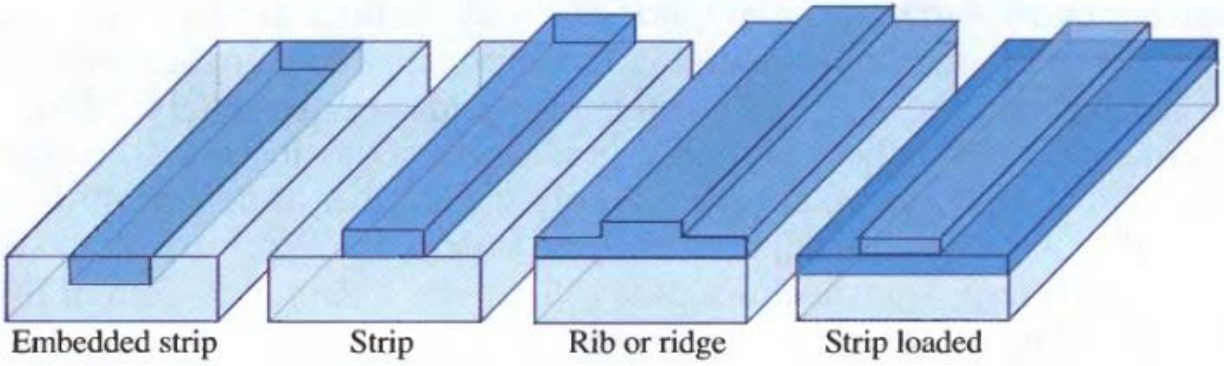

Figure 8.3-3 Various waveguide geometries. The darker the shading, the higher the refractive index.

Bragg-Grating Waveguide as a Photonic Crystal with a Defect Layer

If the upper and lower gratings of a Bragg-grating waveguide are identical, and the slab thickness is comparable to the thickness of the periodic layers constituting the gratings, then the entire medium may be regarded as a 1D periodic structure, i.e., a 1D photonic crystal, but with a **defect**. For example, the device shown in Fig. 8.4-1 is periodic

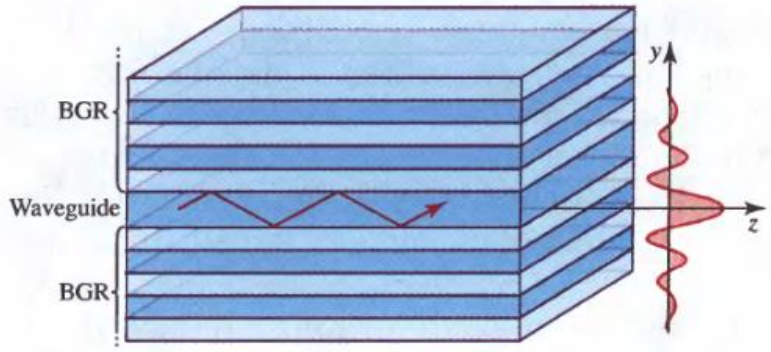

Figure 8.4-1 Planar waveguide made of a dielectric slab sandwiched between two Bragg-grating reflectors (BGR).

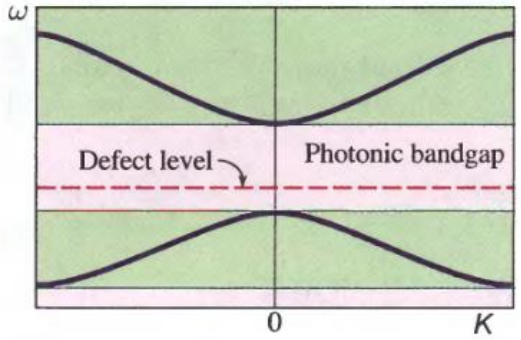

Figure 8.4-2 Dispersion diagram of a photonic crystal with a defect layer.

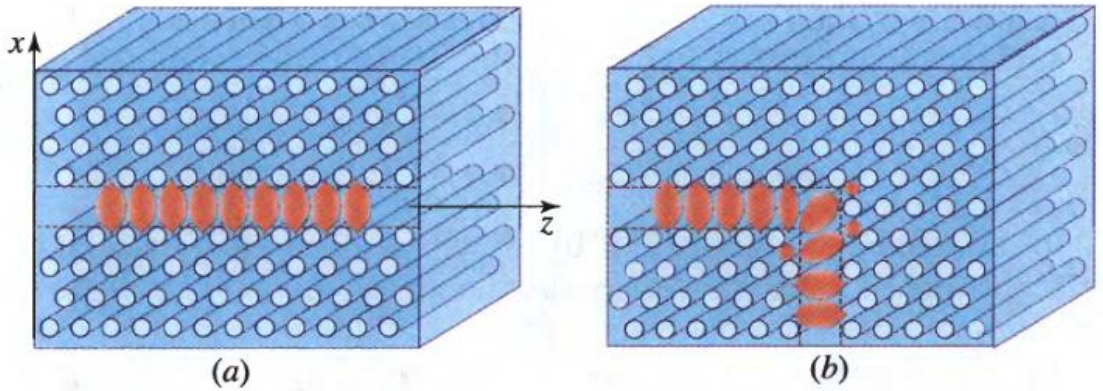

Figure 8.4-3 (a) Propagating mode in a photonic-crystal waveguide. (b) L-shaped photonic-crystal waveguide.

Input Couplers

Light may be coupled into a waveguide by directly focusing it at one end (Fig. 8.5-1). To excite a given mode, the transverse distribution of the incident light $s(y)$ should match that of the mode. The polarization of the incident light must also match that of the desired mode. Because of the small dimensions of the waveguide slab, focusing and alignment are usually difficult and coupling using this method is inefficient.

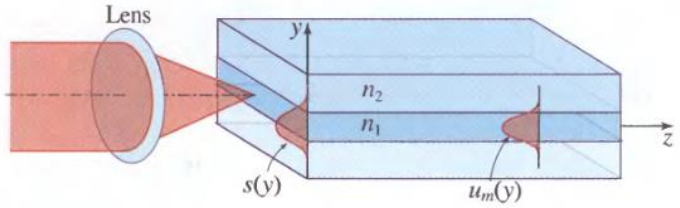

Figure 8.5-1 Coupling an optical beam into an optical waveguide.

Coupling

Input Couplers

Light may be coupled into a waveguide by directly focusing it at one end (Fig. 8.5-1). To excite a given mode, the transverse distribution of the incident light $s(y)$ should match that of the mode. The polarization of the incident light must also match that of the desired mode. Because of the small dimensions of the waveguide slab, focusing and alignment are usually difficult and coupling using this method is inefficient.

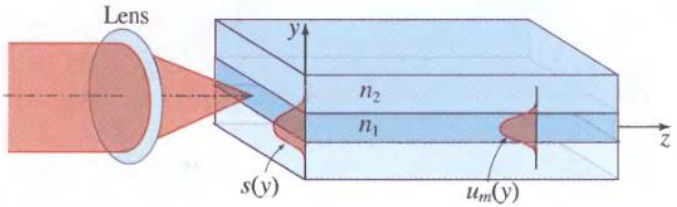

Figure 8.5-1 Coupling an optical beam into an optical waveguide.

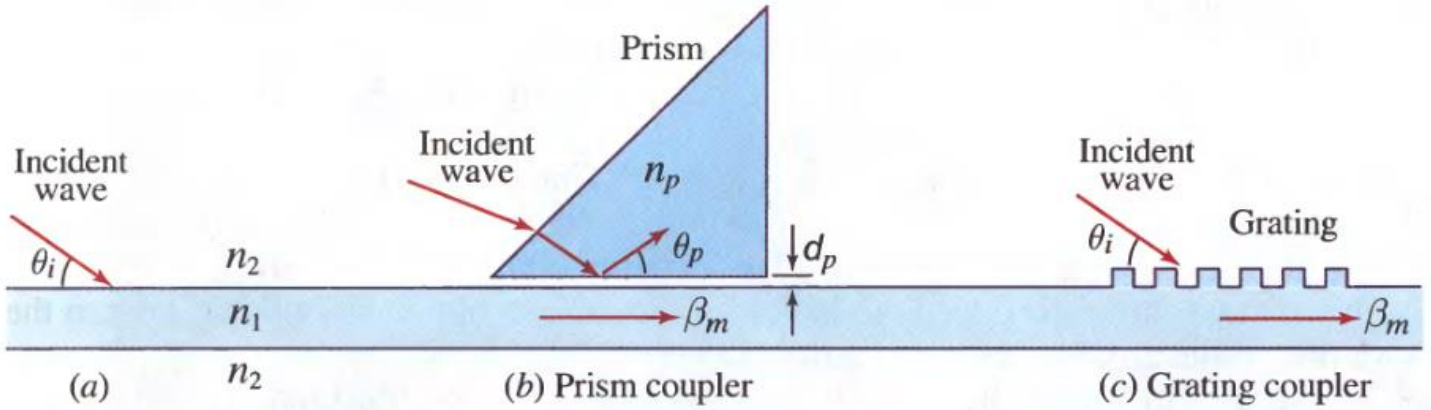

Figure 8.5-4 Prism and grating side couplers.

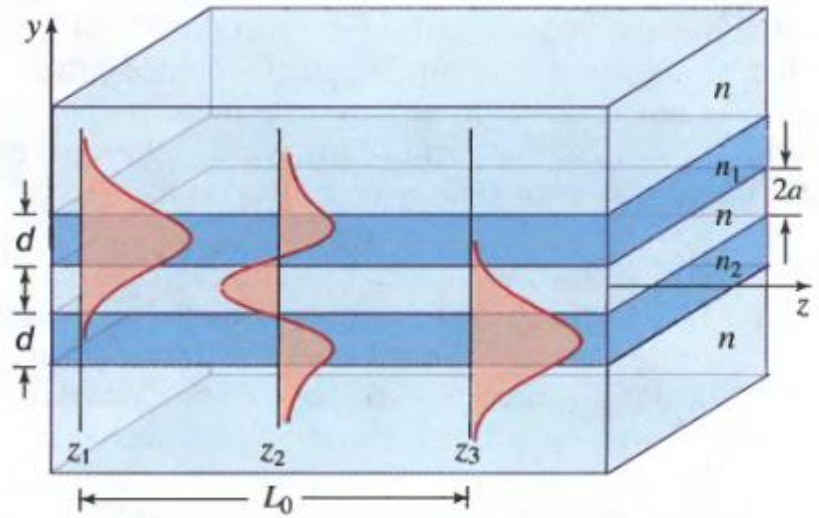

Figure 8.5-5 Coupling between two parallel planar waveguides. At z_1 light is mostly in waveguide 1, at z_2 it is divided equally between the two waveguides, and at z_3 it is mostly in waveguide 2.

Coupled-mode theory

$u_1(y)\exp(-j\beta_1 z)$ and $u_2(y)\exp(-j\beta_2 z)$.

$n_1 = n_2$, $\beta_1 = \beta_2$, and $\Delta\beta = 0$, the
In this case, $\gamma = \mathcal{C}$, $\mathcal{C}_{12} = \mathcal{C}_{21} = \mathcal{C}$,

$$\frac{da_1}{dz} = -j\mathcal{C}_{21}\exp(j\,\Delta\beta\, z)\, a_2(z) \qquad (8.5\text{-}4a)$$

$$\frac{da_2}{dz} = -j\mathcal{C}_{12}\exp(-j\,\Delta\beta\, z)\, a_1(z), \qquad (8.5\text{-}4b)$$

Coupled-Mode Equations

$$P_1(z) = P_1(0)\cos^2 \mathcal{C}z$$
$$P_2(z) = P_1(0)\sin^2 \mathcal{C}z.$$

Optical coupler

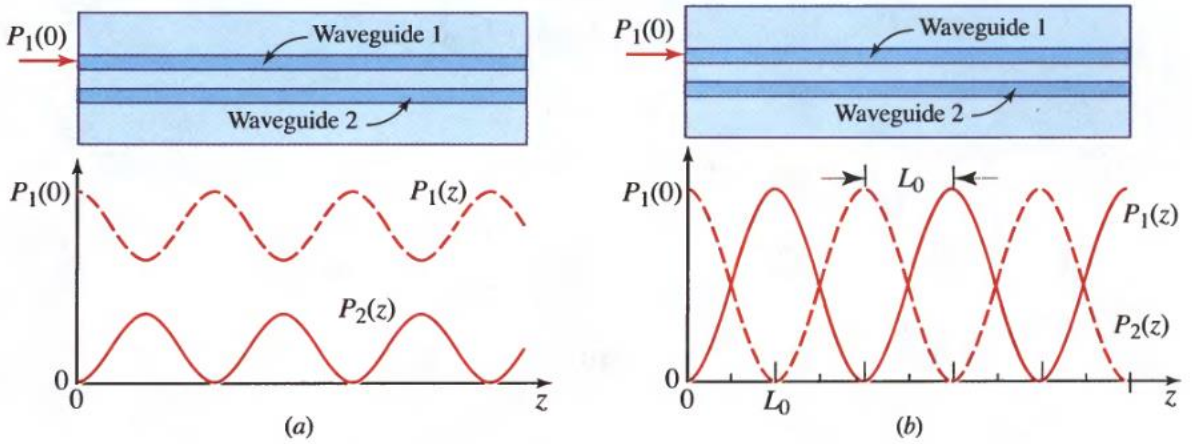

Figure 8.5-6 Periodic exchange of power between waveguides 1 and 2: (a) Phase mismatched case; (b) Phase matched case.

We thus have a device capable of coupling any desired fraction of optical power from one waveguide into another. At a distance $z = L_0 = \pi/2\mathcal{C}$, called the **coupling length** or the **transfer distance**, the power is transferred completely from waveguide 1 into waveguide 2 [Fig. 8.5-7(a)]. At a distance $L_0/2$, half the power is transferred, so that the device acts as a 3-dB coupler, i.e., a 50/50 beamsplitter [Fig. 8.5-7(b)].

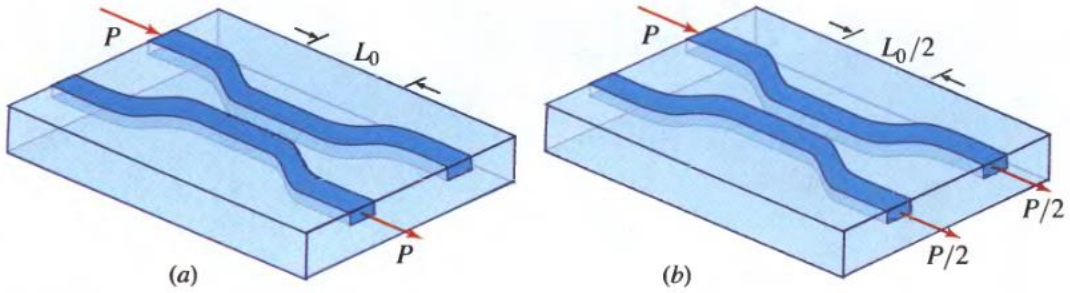

Figure 8.5-7 Optical couplers: (a) switching power from one waveguide to another; (b) a 3-dB coupler.

Resonator Optics

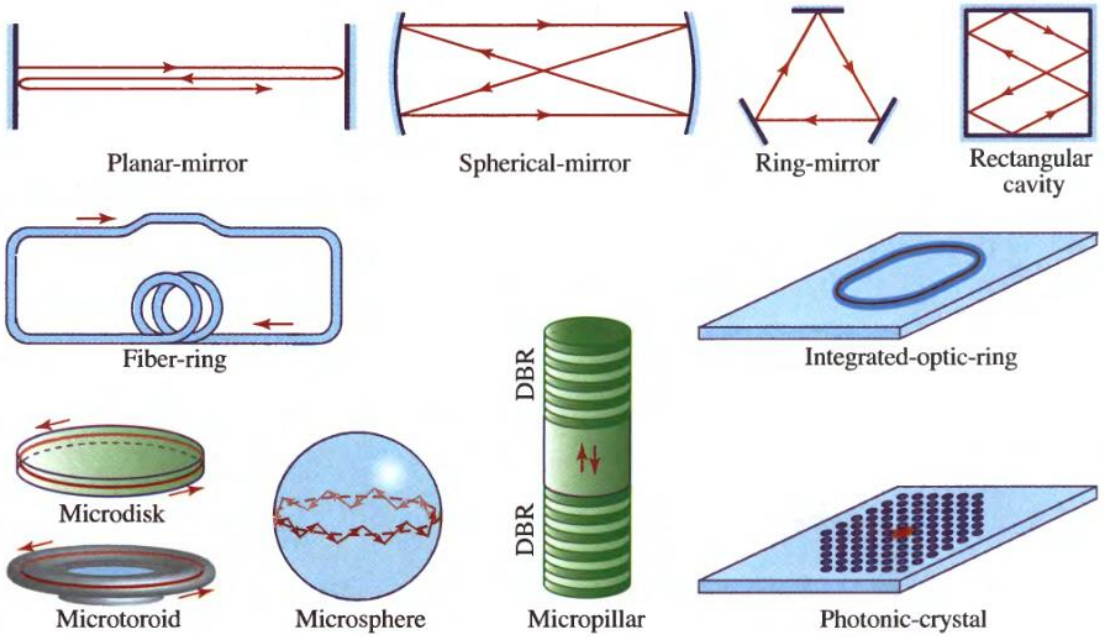

Figure 10.0-1 Storage of light in optical resonators via: multiple reflections from mirrors; propagation though closed-loop optical fibers and integrated-optic waveguides; whispering-gallery mode reflections near the surface of disks, toroids, and spheres; reflections from periodic structures such as Bragg gratings; and defects in photonic crystals.

Quality Factor Q

The **quality factor** Q is often used to characterize electrical resonance circuits and microwave resonators. This parameter is defined as

$$Q = 2\pi \frac{\text{stored energy}}{\text{energy loss per cycle}}. \qquad (10.1\text{-}32)$$

Microcavities

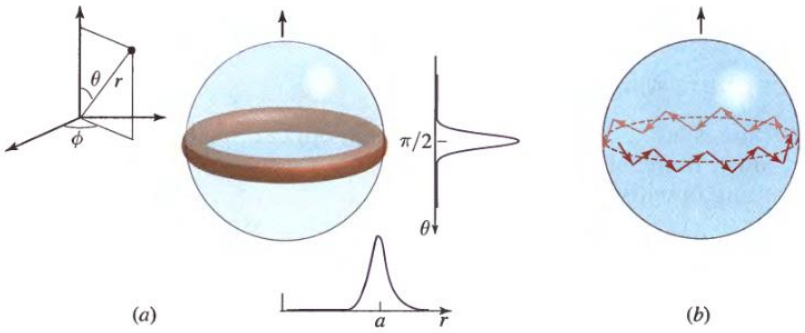

Figure 10.4-3 (*a*) Whispering-gallery mode in a microsphere resonator. (*b*) Ray model of the whispering-gallery mode.

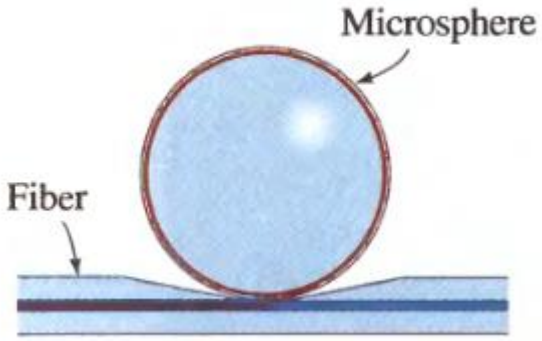

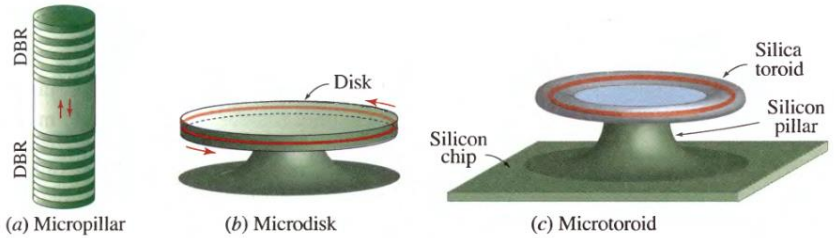

Figure 10.4-2 Micropillar, microdisk, and microtoroid resonators.

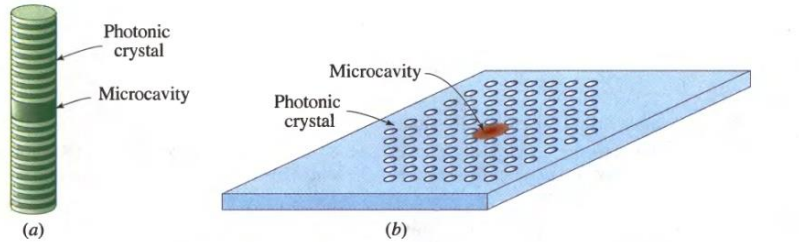

Figure 10.4-5 Photonic-crystal microresonators. (*a*) The micropillar resonator as a 1D photonic crystal in which the microresonator acts as a defect. (*b*) A 2D photonic-crystal resonator may be fabricated by drilling holes in a dielectric slab at the points of a planar hexagonal lattice; a missing hole serves as the microcavity.

Quality Factor Q

The **quality factor** Q is often used to characterize electrical resonance circuits and microwave resonators. This parameter is defined as

$$Q = 2\pi \frac{\text{stored energy}}{\text{energy loss per cycle}}. \tag{10.1-32}$$

Quality Factor

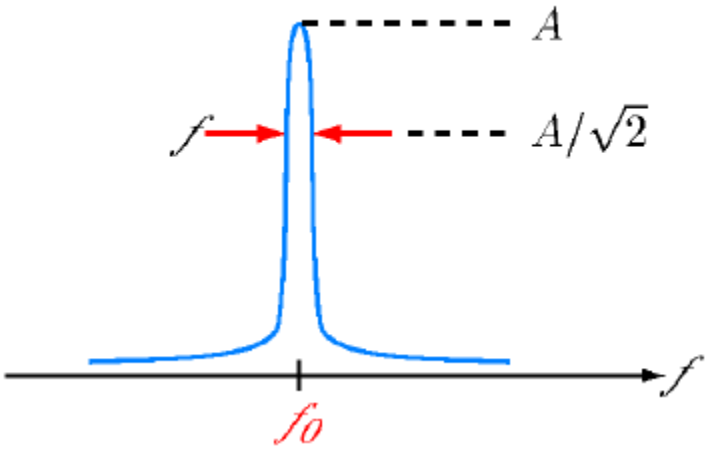

- $Q \approx \frac{f_{mnp}}{\Delta f}$

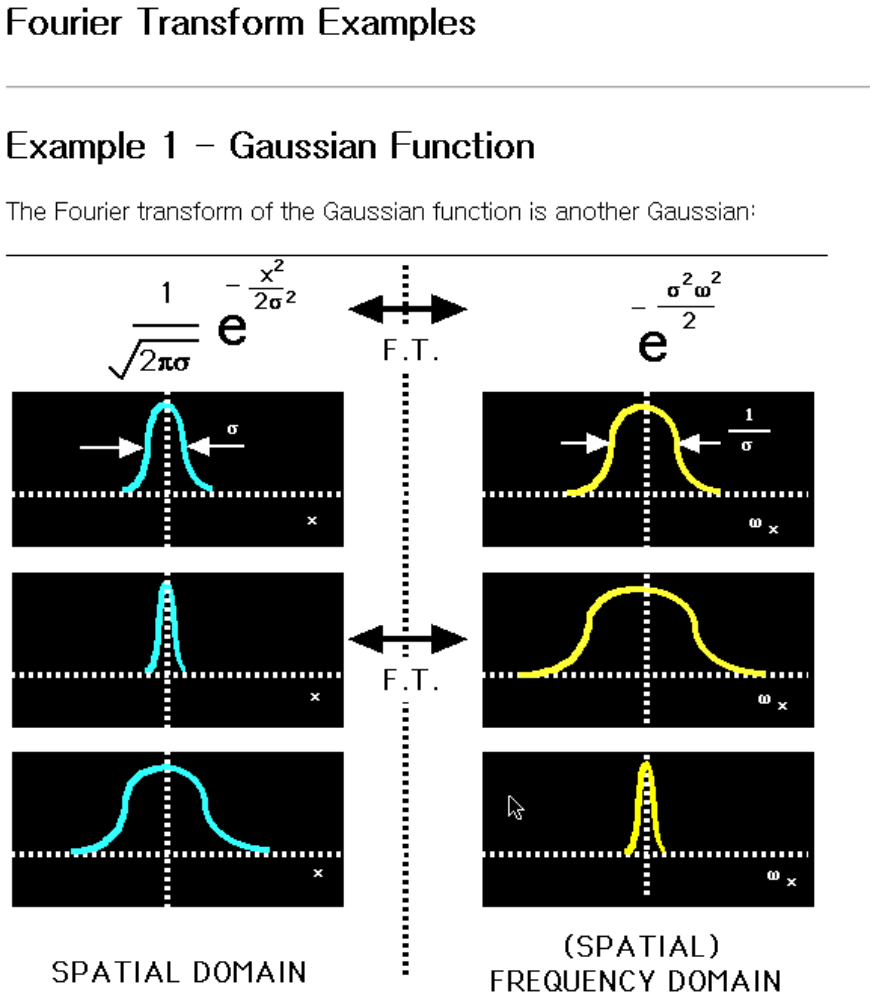

Laser

http://www.youtube.com/watch?v=R_QOWbkc7UI

http://www.youtube.com/watch?v=kNJyBienF-4&feature=related

http://www.youtube.com/watch?v=I65EcfBFIrU

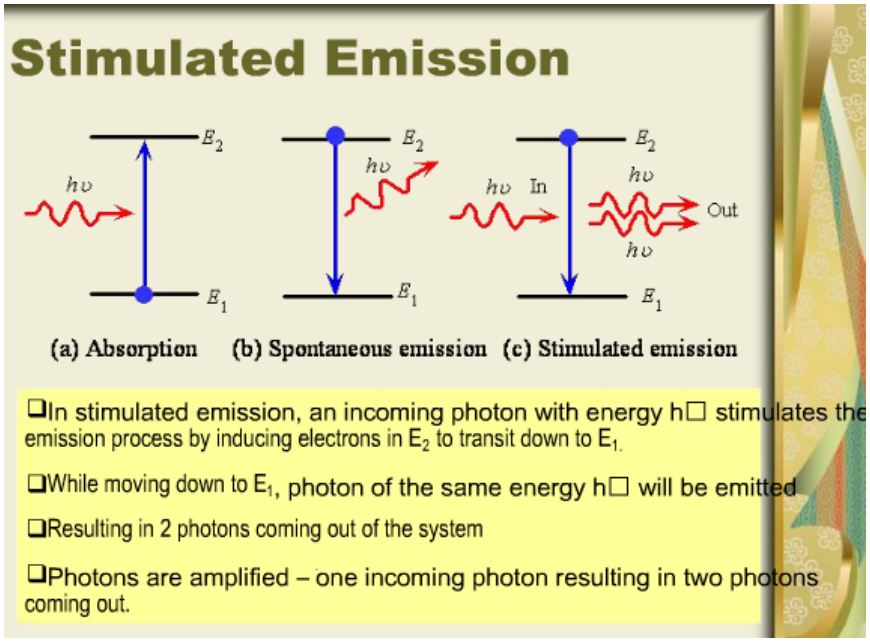

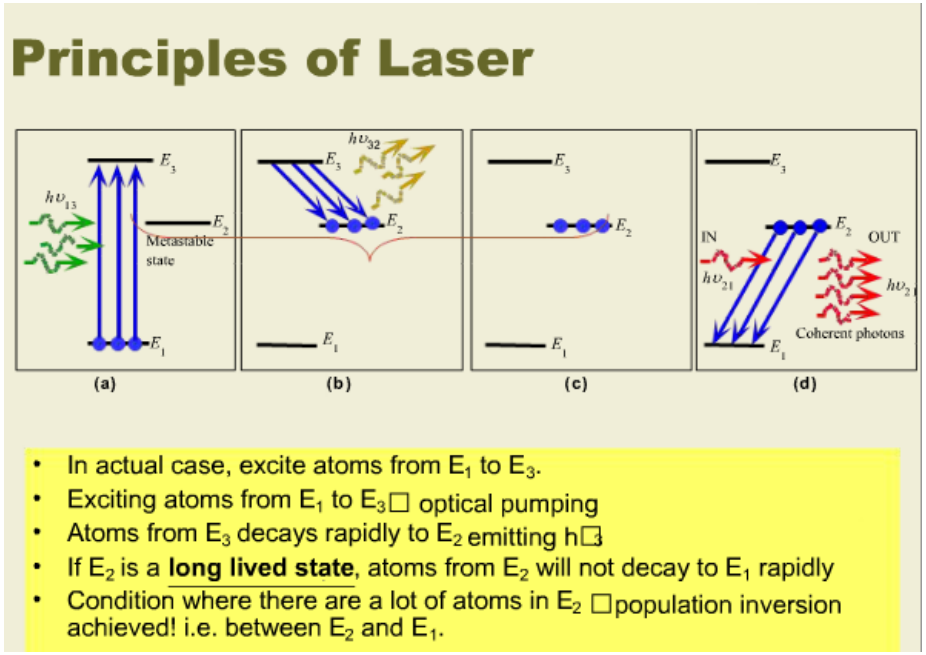

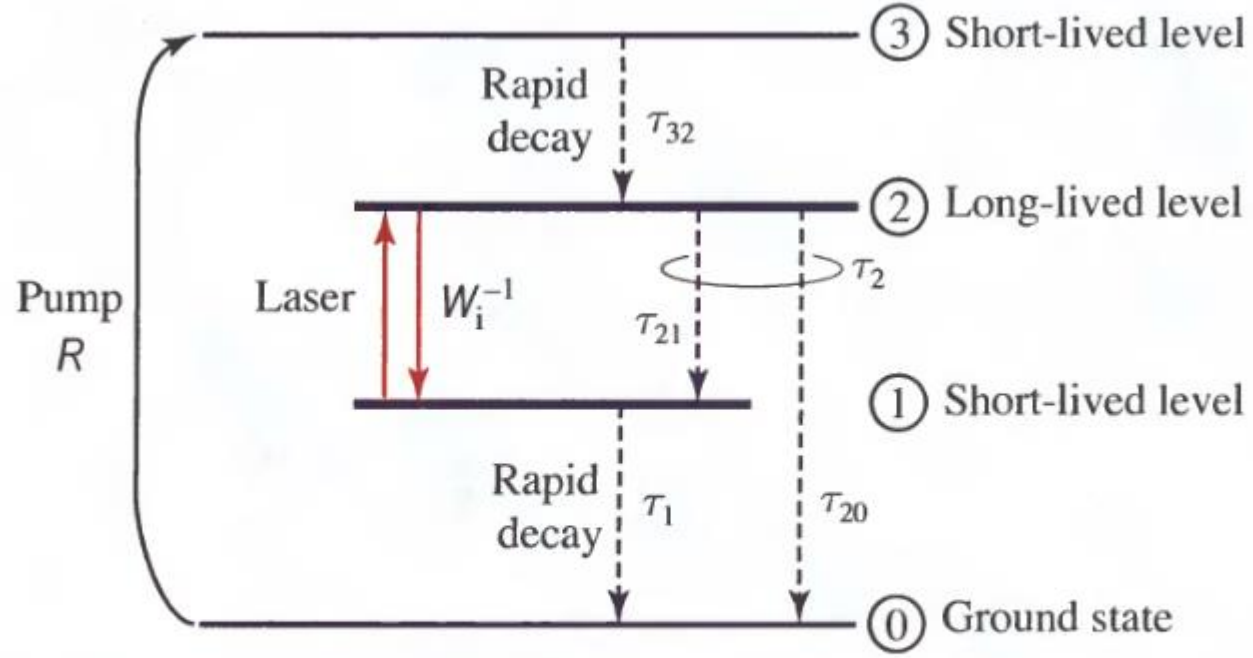

Figure 14.2-6 Energy levels and decay rates for a four-level system. The four levels are drawn from a multitude of levels (not shown). It is assumed that the rate of pumping into level 3, and out of level 0, are the same.

Three-Level Pumping

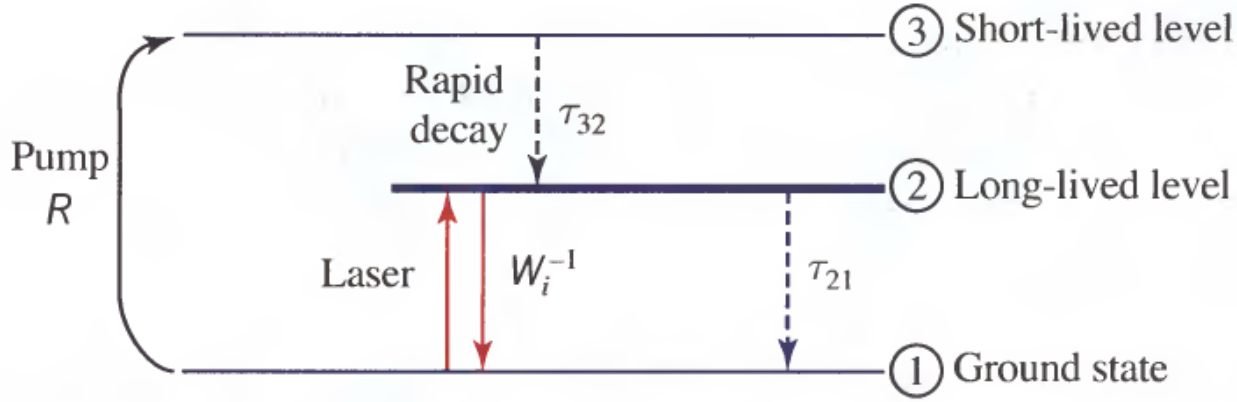

Figure 14.2-7 Energy levels and decay rate for a three-level system. A multitude of other energy levels exist, but they are not germane to the considerations at hand. It is assumed that the rate of pumping into level 3 is the same as the rate of pumping out of level 1.

Pumping Methods

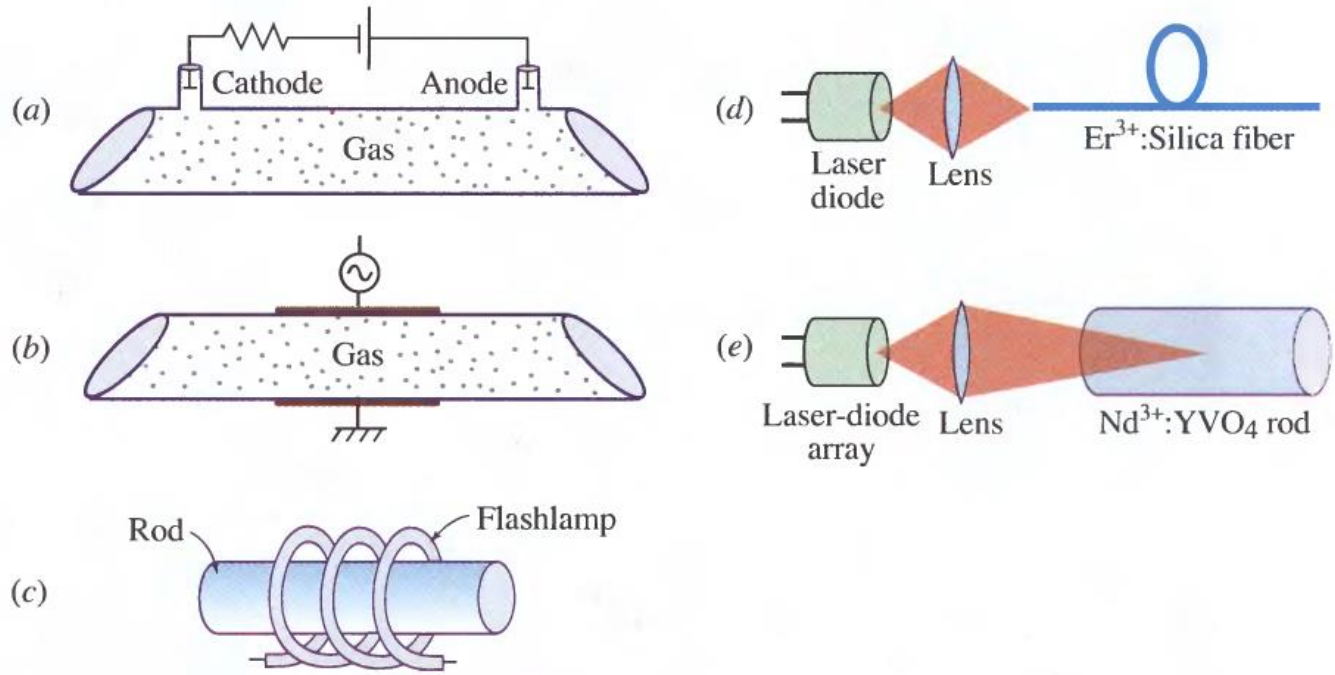

Figure 14.2-8 Examples of electrical and optical pumping. (*a*) Direct current (dc) is often used to pump gas lasers. The current may be passed either along the laser axis, creating a longitudinal discharge, or transverse to it. (*b*) Radio-frequency (RF) discharge currents are also used for pumping gas lasers. (*c*) Xe flashlamps or Kr CW arc lamps are useful for optically pumping ruby and rare-earth solid-state lasers. (*d*) Semiconductor laser diodes are often used for pumping Er^{3+}:silica fiber laser amplifiers. (*e*) An array of laser diodes is generally used to optically pump Nd^{3+}:YVO_4 lasers.

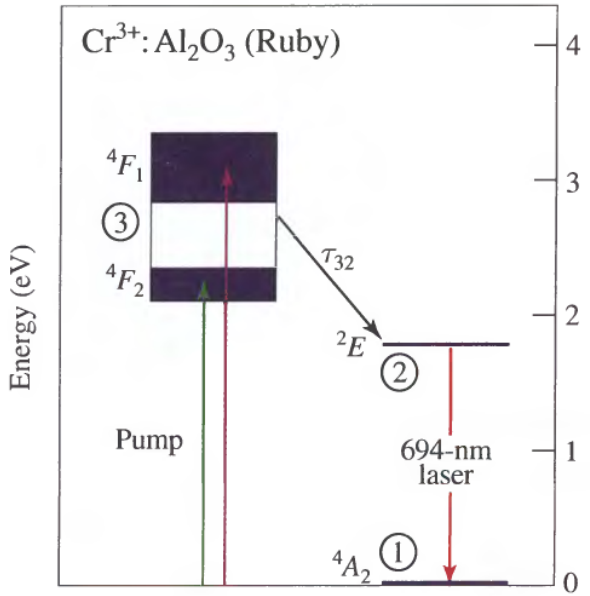

Figure 14.3-1 Relevant energy levels for the $^2E \rightarrow {}^4A_2$ red ruby-laser transition at 694.3 nm. The three interacting levels are indicated by encircled numbers.

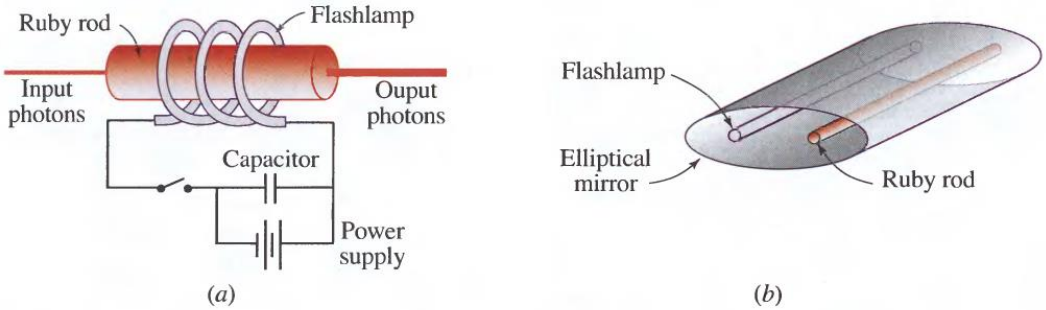

Figure 14.3-2 Ruby laser-amplifier configurations. (*a*) Geometry used for the first laser oscillator built by Maiman in 1960 (see page 567 of Chapter 15). (*b*) High-efficiency pumping geometry using a linear flashlamp in a reflecting elliptical cylinder.

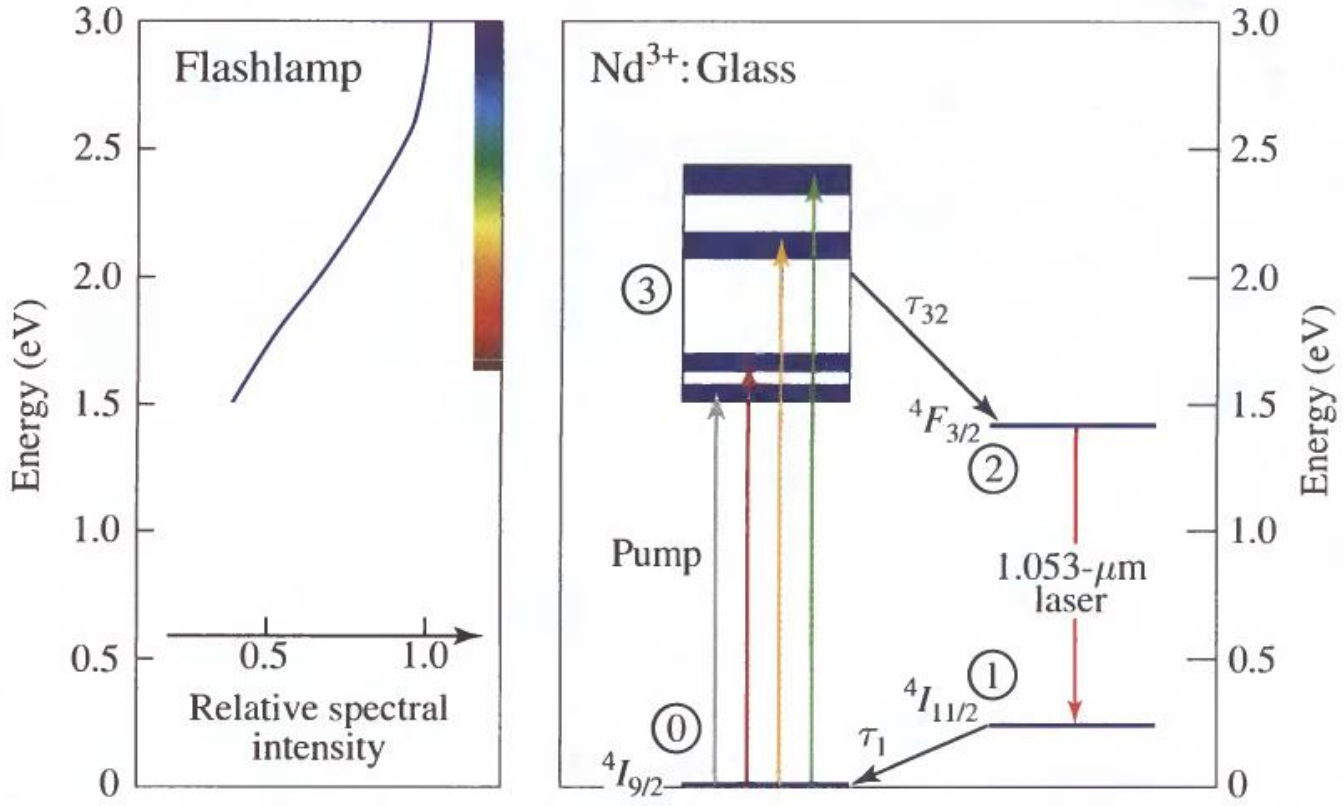

Figure 14.3-3 Left: Spectral profile of the broadband Xe flashlamp emission used to pump the neodymium-doped glass laser amplifiers at the National Ignition Facility (NIF). Right: Relevant energy levels for the ${}^4F_{3/2} \rightarrow {}^4I_{11/2}$ laser transition at 1.053 μm in neodymium-doped phosphate glass (Schott LG-770). The four interacting energy levels are indicated by encircled numbers.

$$0 \le \left(1 + \frac{d}{R_1}\right)\left(1 + \frac{d}{R_2}\right) \le 1. \qquad (10.2\text{-}5)$$

It is convenient to write this condition in terms of the quantities $g_1 = 1 + d/R_1$ and $g_2 = 1 + d/R_2$, which are known as the **g parameters**:

$$\boxed{0 \le g_1\, g_2 \le 1.} \qquad (10.2\text{-}6)$$

Confinement Condition

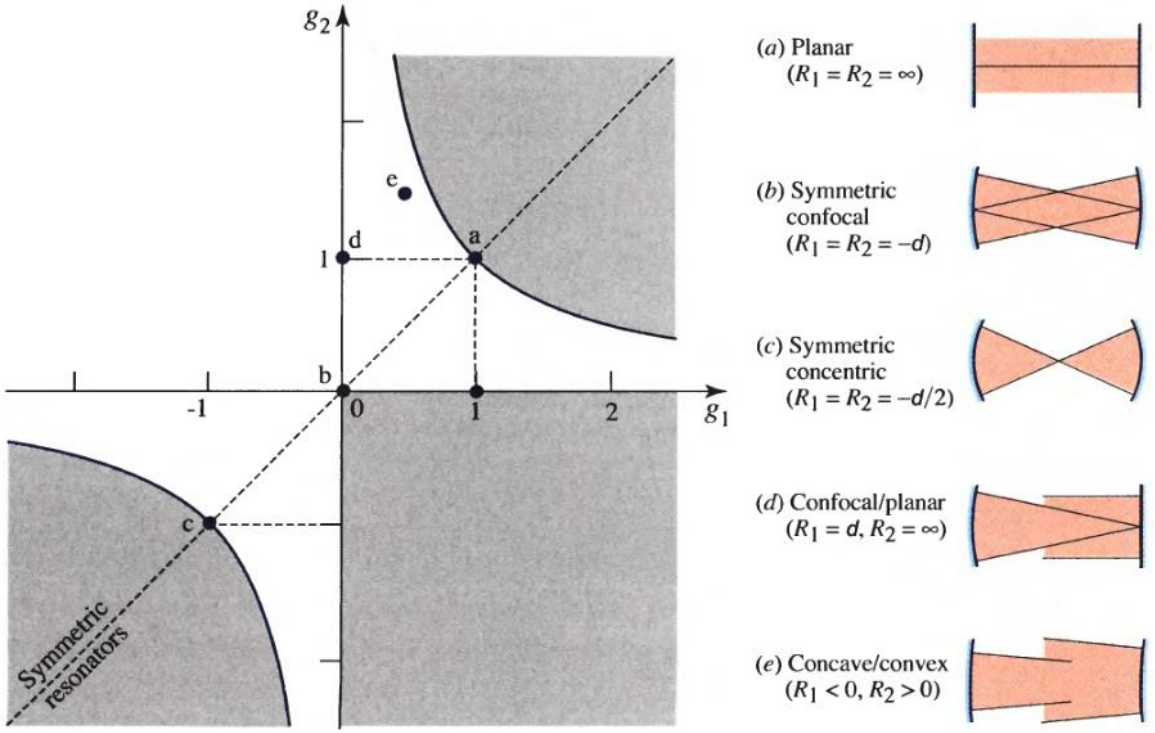

Figure 10.2-3 Resonator stability diagram. A spherical-mirror resonator is stable if the parameters $g_1 = 1 + d/R_1$ and $g_2 = 1 + d/R_2$ lie in the unshaded regions, which are bounded by the lines $g_1 = 0$ and $g_2 = 0$, and the hyperbola $g_2 = 1/g_1$. R is negative for a concave mirror and positive for a convex mirror. Commonly used resonator configurations are indicated by letters and sketched at the right. All symmetric resonators lie along the line $g_2 = g_1$.

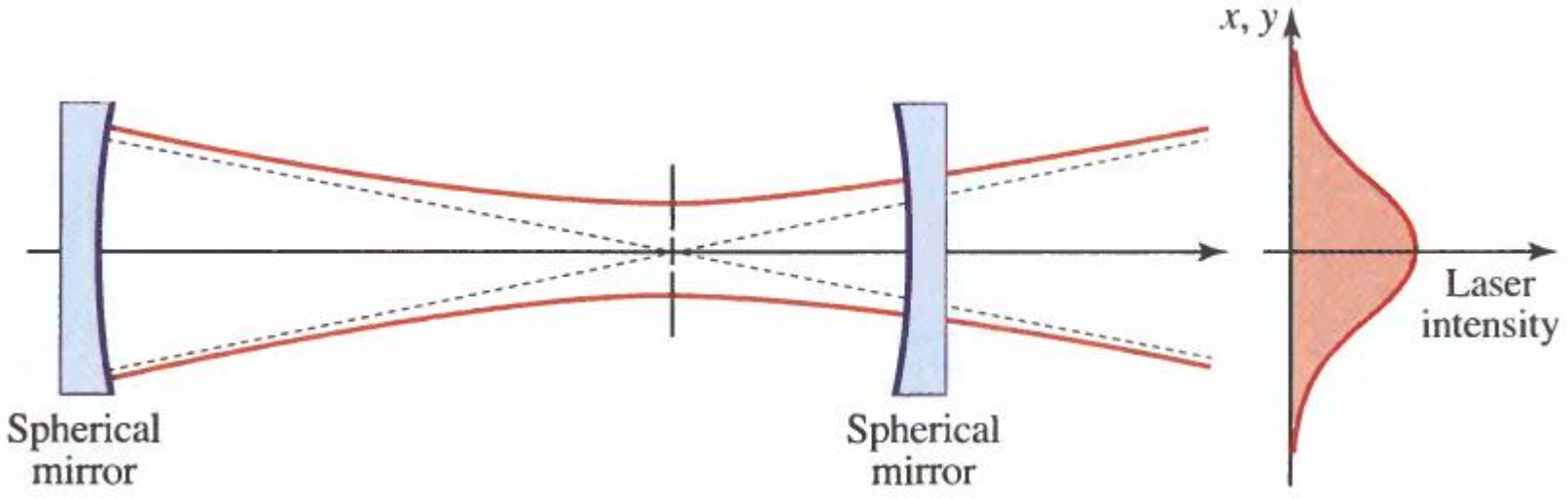
x, y
Spherical mirror
Spherical mirror
Laser intensity

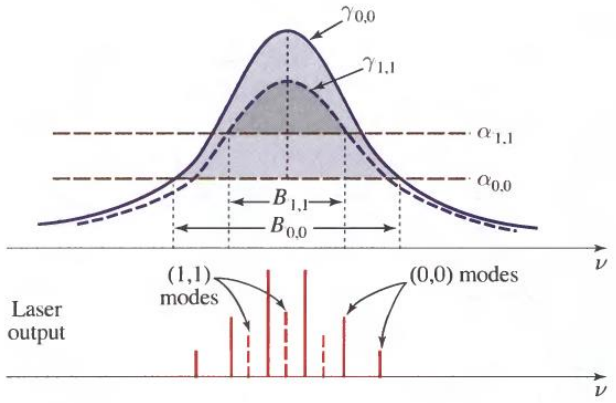
$\gamma_{0,0}$
$\gamma_{1,1}$
$\alpha_{1,1}$
$\alpha_{0,0}$
$B_{1,1}$
$B_{0,0}$
ν
(1,1) modes
(0,0) modes
Laser output
ν

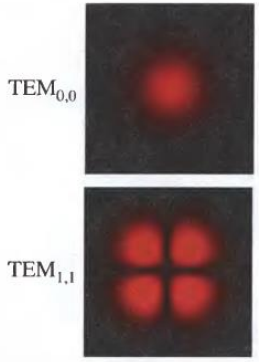
$TEM_{0,0}$
$TEM_{1,1}$

Erbium-Doped Silica Fiber

Optical fiber amplifiers (OFAs)

erbium-doped fiber amplifiers (EDFAs)

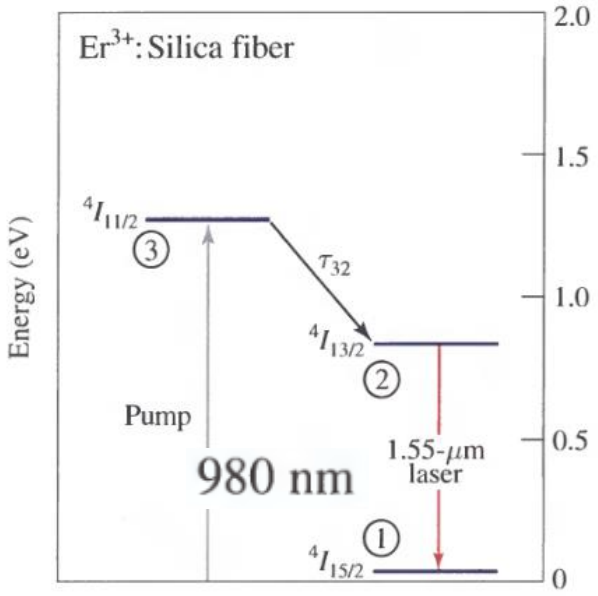

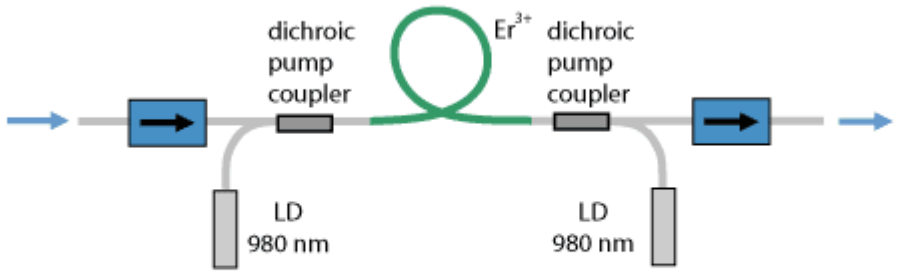

Figure 1: Schematic setup of a simple erbium-doped fiber amplifier. Two laser diodes (LDs) provide the pump power for the erbium-doped fiber. The pump light is injected via dichroic fiber couplers. Pig-tailed optical isolators reduce the sensitivity of the device to back-reflections.

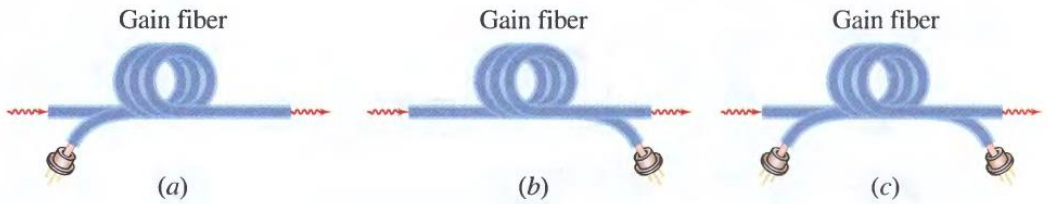

Figure 14.3-5 Longitudinal pumping of a fiber laser amplifier. The pumping may be (a) in the forward direction; (b) in the backward direction; or (c) bidirectional. Er^{3+}: silica-fiber amplifiers are often pumped by strained InGaAs laser diodes operated at $\lambda_o = 980$ nm. Raman silica fiber amplifiers, discussed in Sec. 14.3D, can also be pumped by InGaAsP laser diodes operated at a wavelength about 100 nm below that desired for amplification; however, Raman fiber laser pumping is common.

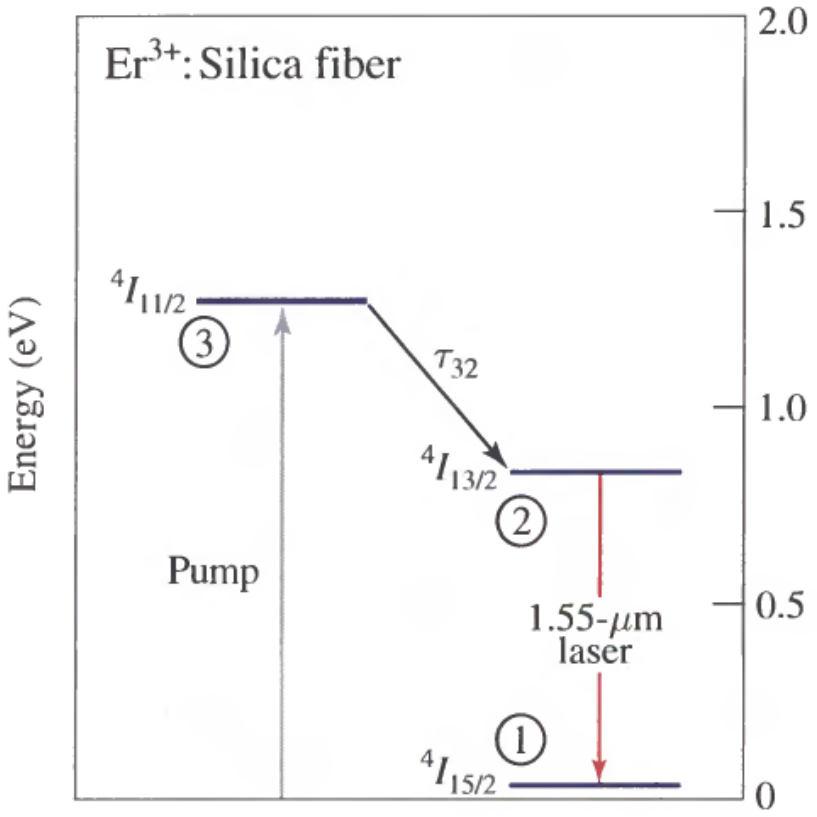

Figure 14.3-6 Schematic of energy-level manifolds for the Er^{3+}: silica fiber ${}^4I_{13/2} \rightarrow {}^4I_{15/2}$ laser transition in the vicinity of 1550 nm. The erbium-doped silica-fiber system behaves as a three-level laser at $T = 300°$ K. The three interacting levels are indicated by encircled numbers. The system can also be made to behave as a four-level laser in the vicinity of 2.9 μm on the ${}^4I_{11/2} \rightarrow {}^4I_{13/2}$ transition.

Single Mode lasing

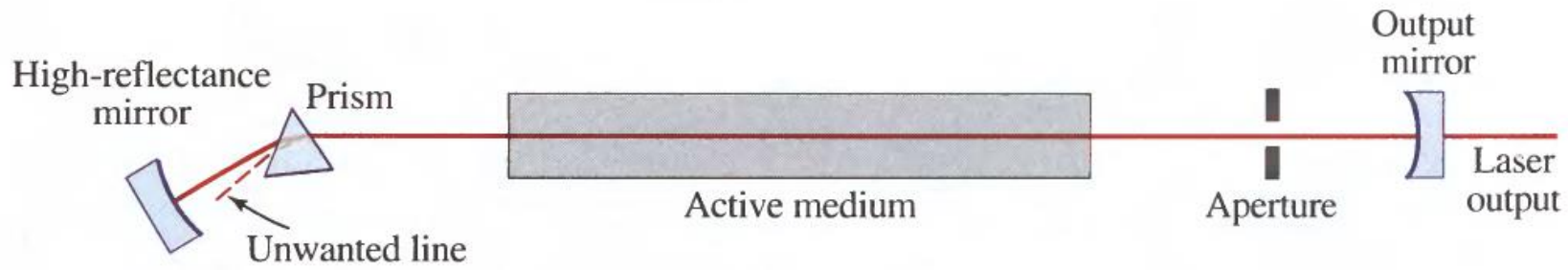

pp589

Homogeneously Broadened Medium

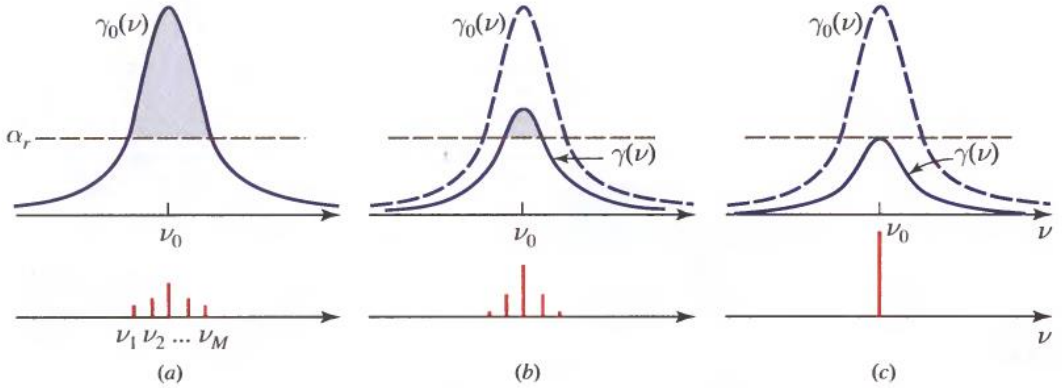

Inhomogeneously Broadened Medium

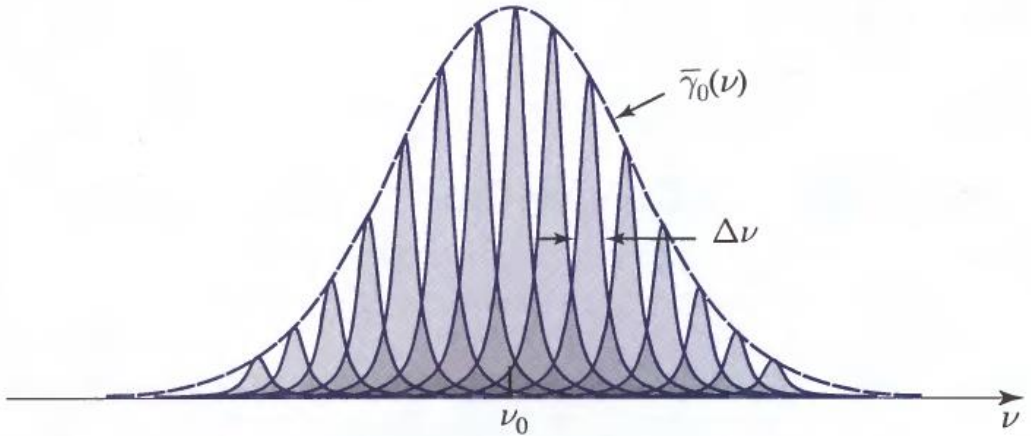

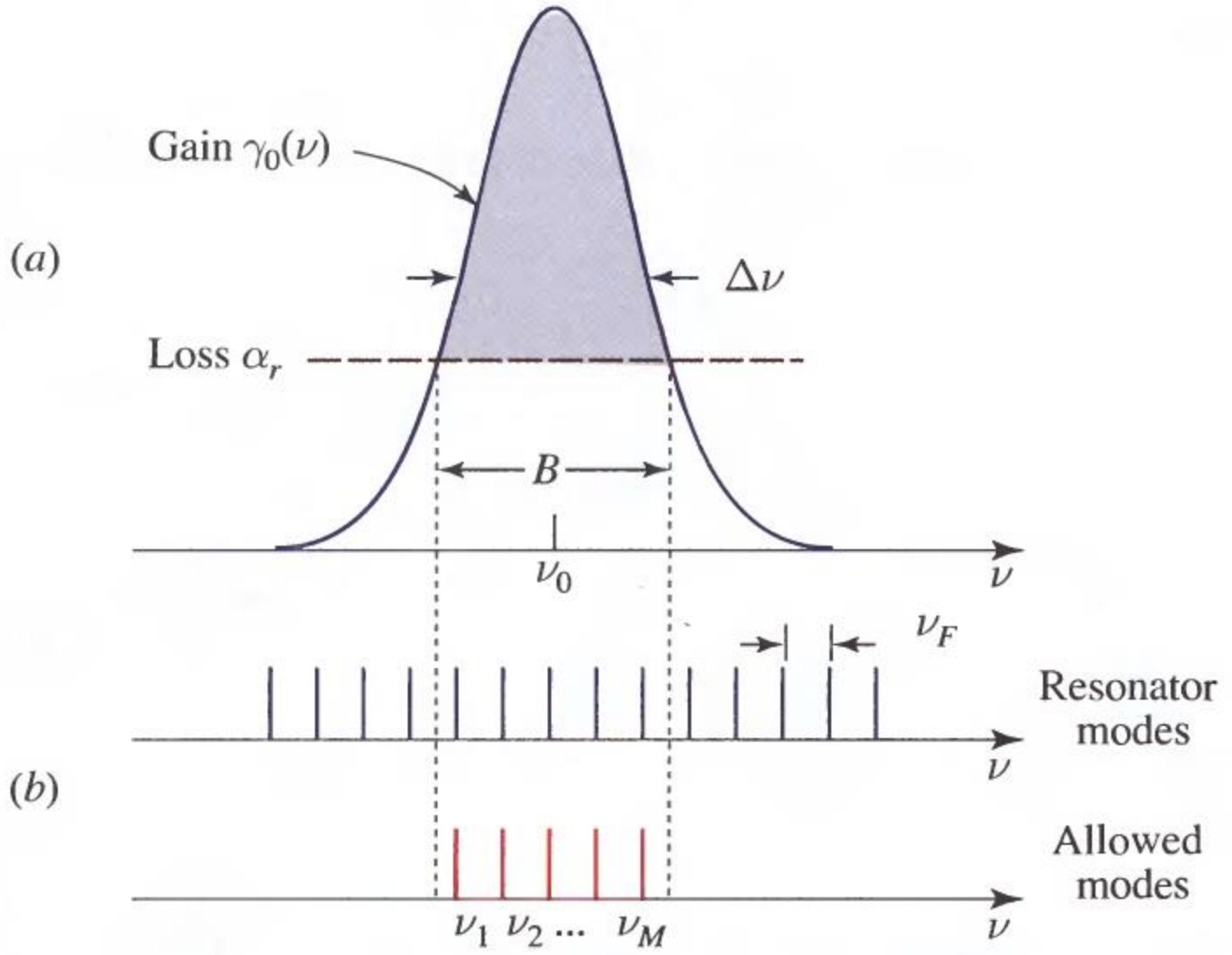
Gain $\gamma_0(\nu)$
(a)
$\Delta\nu$
Loss α_r
B
ν_0
ν
ν_F
Resonator modes
ν
(b)
Allowed modes
ν_1 ν_2 ... ν_M
ν

Homogeneously Broadened Medium

Single mode prefer except **spatial hole burning.**

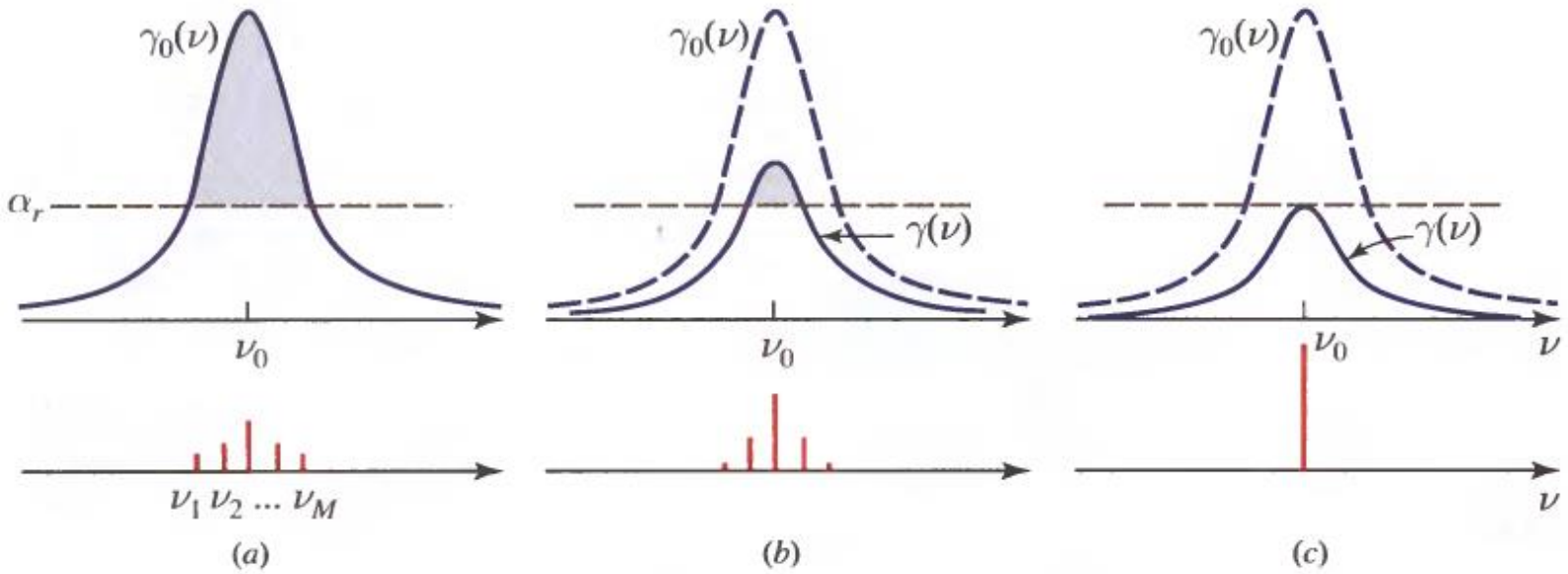

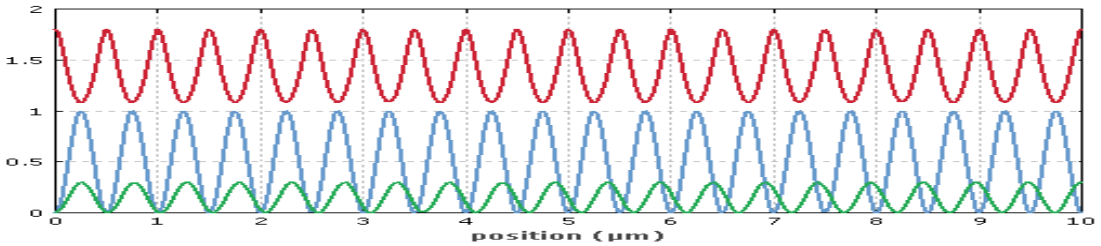

TE/ TM
mode generation
(Brewster angle)

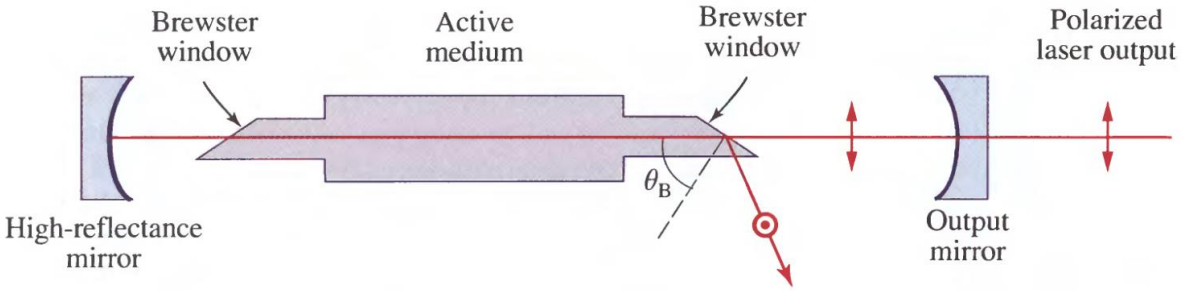

Figure 15.2-13 The use of Brewster windows in a gas laser provides a linearly polarized laser beam. Light polarized in the plane of incidence (the TM wave) is transmitted without reflection loss through a window placed at the Brewster angle. The orthogonally polarized (TE) mode suffers reflection loss and therefore does not oscillate.

Single longitudinal
mode selection
(Etalon)

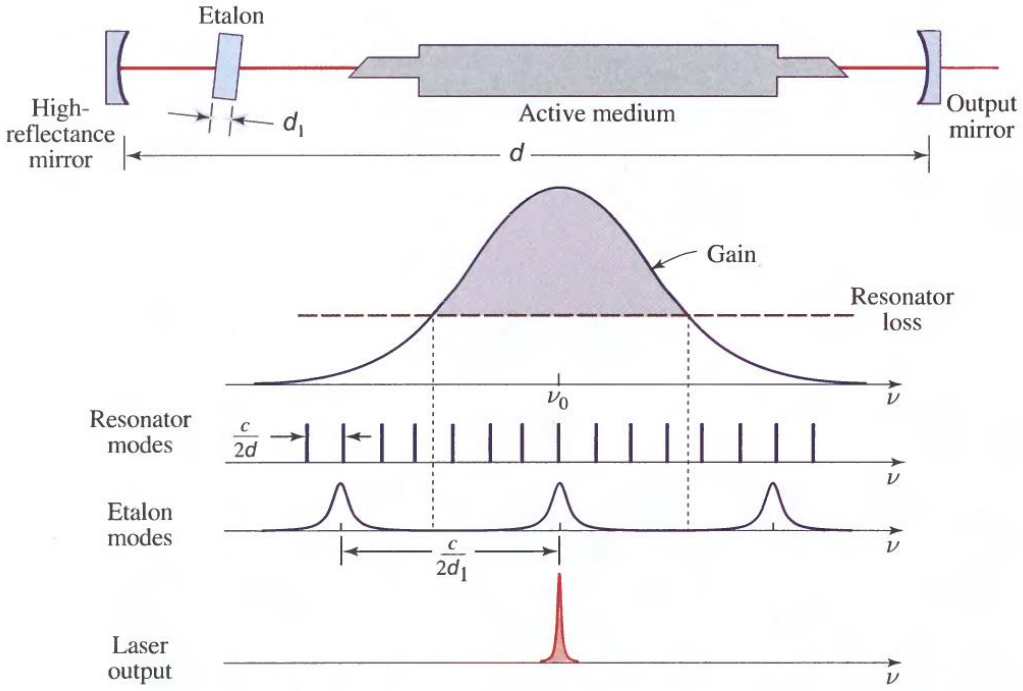

Figure 15.2-14 Longitudinal mode selection by the use of an intracavity etalon. Oscillation occurs at frequencies where a mode of the resonator coincides with an etalon mode; both must, of course, lie within the spectral window where the gain of the medium exceeds the loss.

Pulse generation

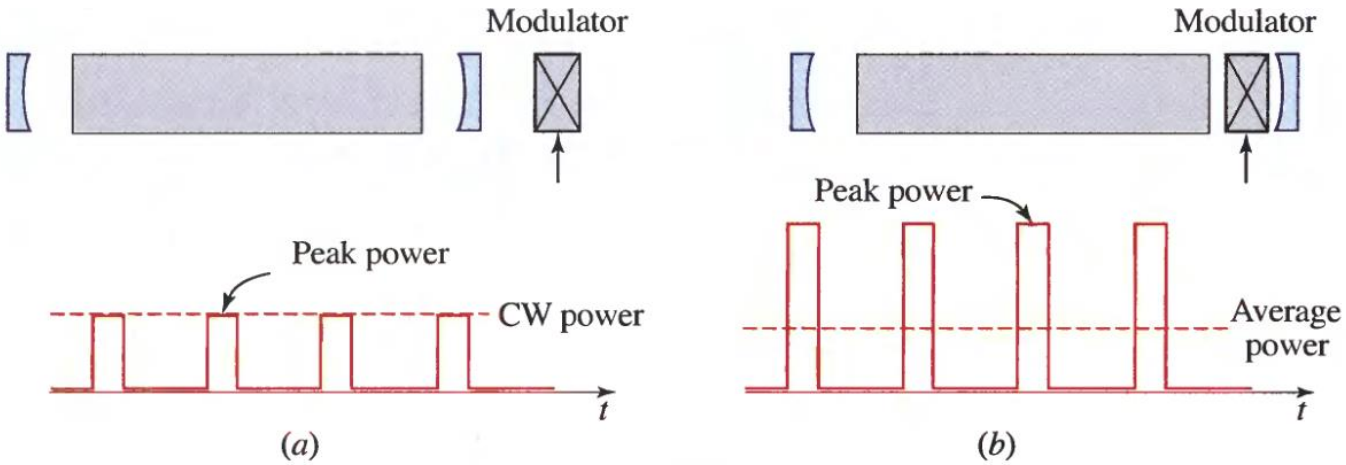

Figure 15.4-1 Comparison of pulsed laser outputs achievable with (*a*) an external modulator, and (*b*) an internal modulator.

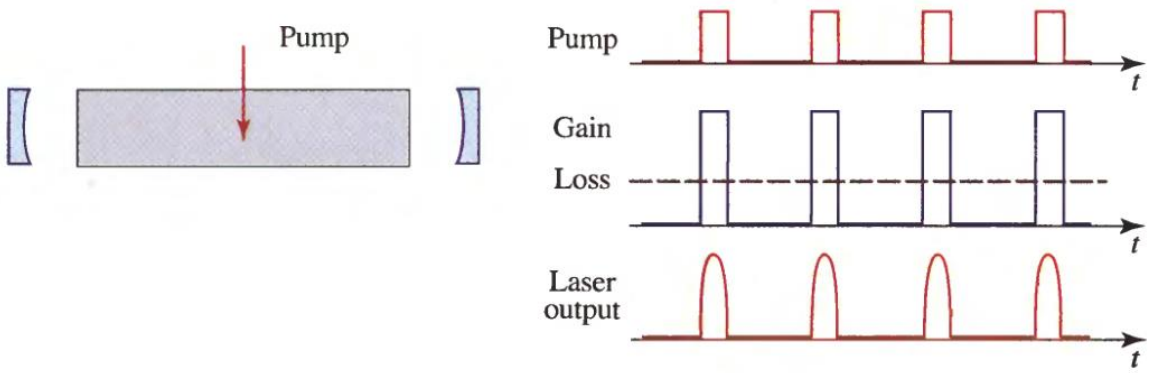

Figure 15.4-2 Gain switching.

Pulse generation

Q-switching

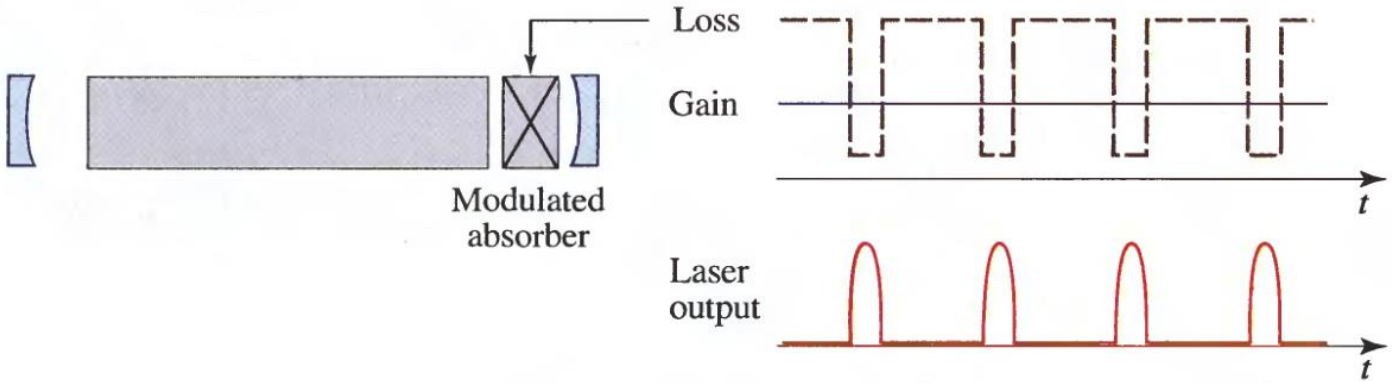

Figure 15.4-3 Q-switching.

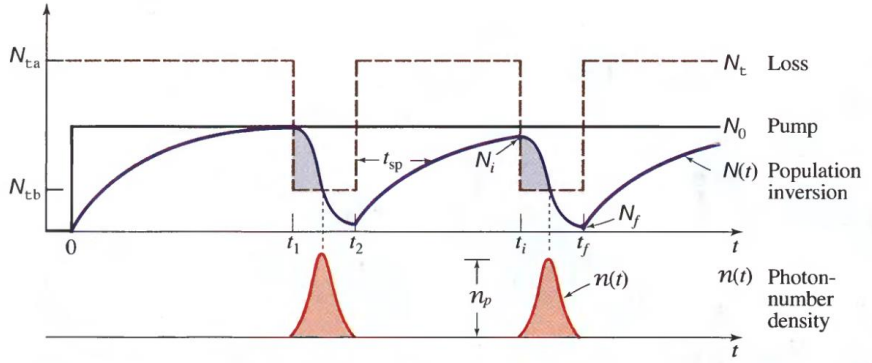

Figure 15.4-6 Operation of a Q-switched laser. Variation of the population threshold N_t (which is proportional to the resonator loss), the pump parameter N_0, the population difference $N(t)$, and the photon number $n(t)$.

$$\sin\theta = \frac{\lambda}{2\Lambda}, \tag{19.0-1}$$

Bragg Condition

where λ is the wavelength of light in the medium (see Exercise 2.5-3). This form of light–sound interaction is known as **Bragg diffraction**, Bragg reflection, or Bragg scattering. The device that effects it is known as a Bragg reflector, a Bragg deflector, or a **Bragg cell**.

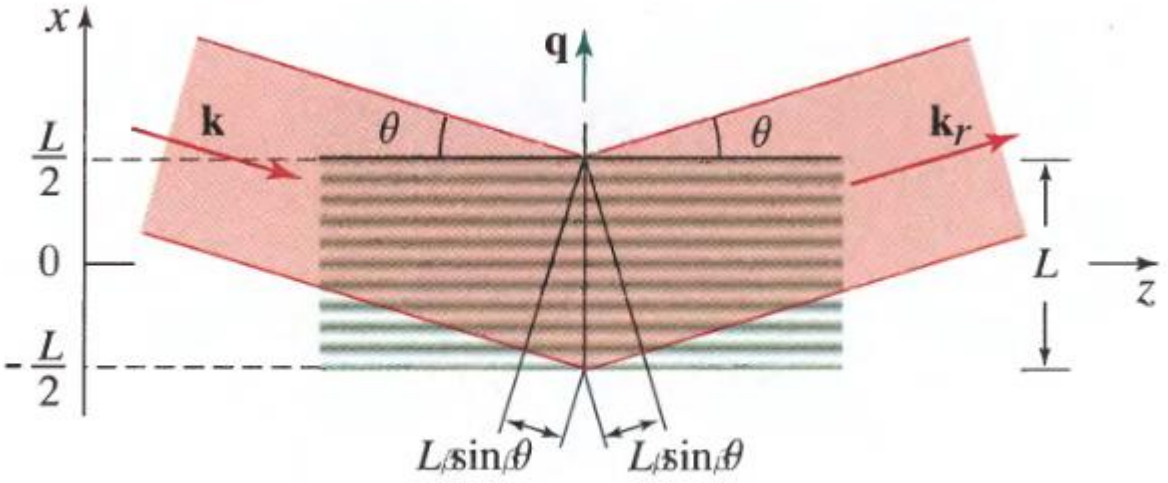

Figure 19.1-1 Reflections from layers of an inhomogeneous medium.

Modelocking

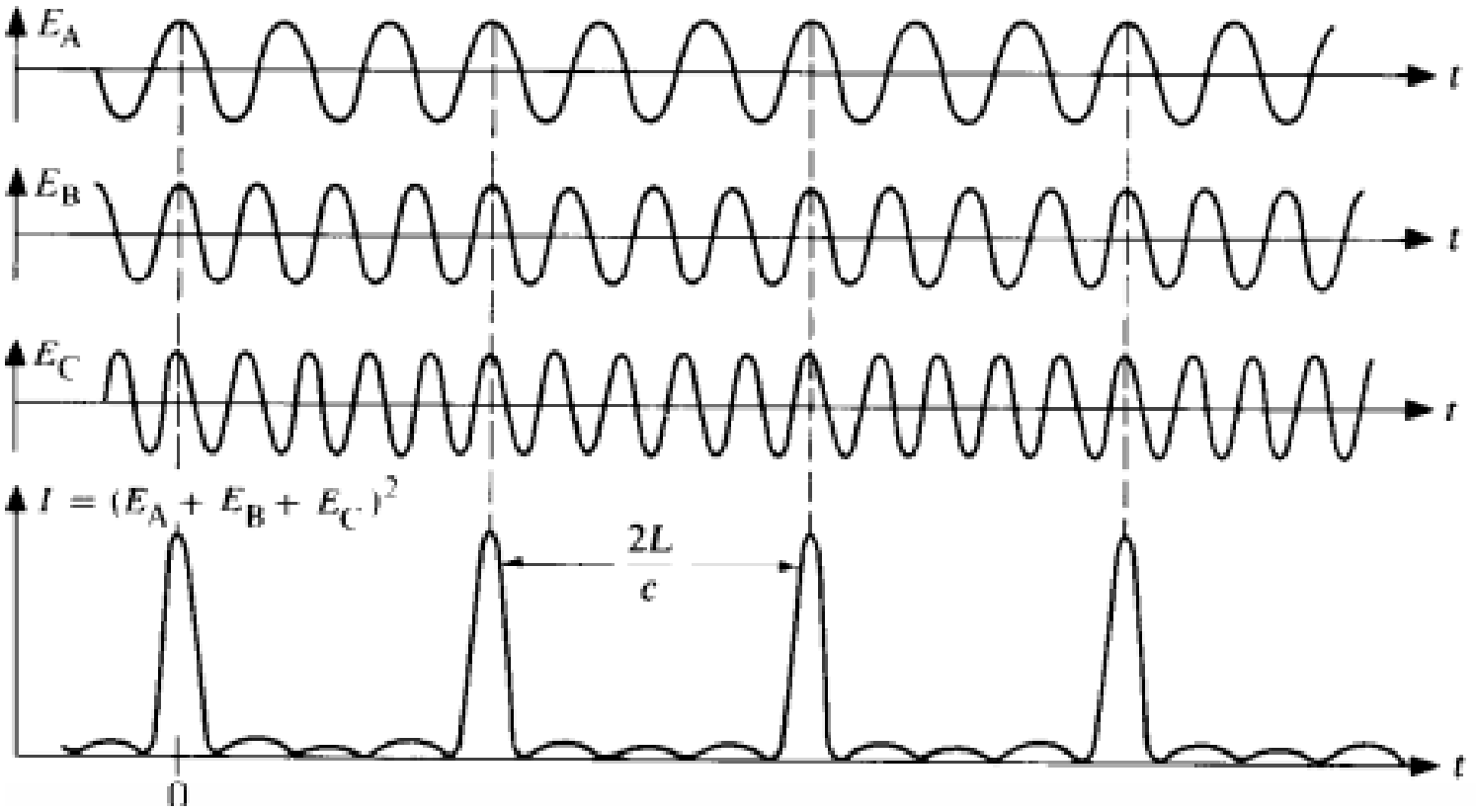

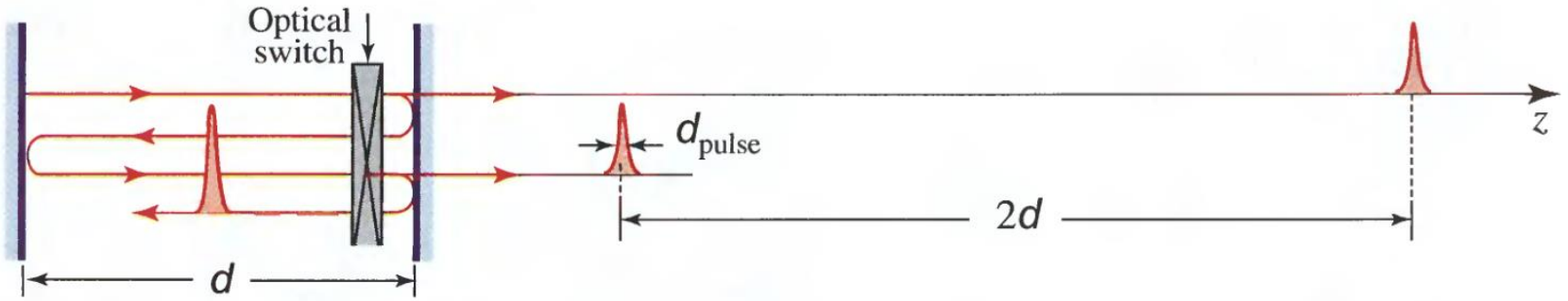

Figure 15.4-10 The mode-locked laser pulse reflects back and forth between the mirrors of the resonator. Each time it reaches the output mirror it transmits a short optical pulse. The transmitted pulses are separated by the distance $2d$ and travel with velocity c. The switch opens only when the pulse reaches it and only for the duration of the pulse. The periodic pulse train is therefore unaffected by the presence of the switch. Other wave patterns, however, suffer losses and are not permitted to oscillate.

Table 15.4-2 Typical pulse durations for a number of mode-locked lasers subject to homogeneous (H) and inhomogeneous (I) broadening.

Laser Medium		Transition Linewidth[a] $\Delta\nu$	Calculated Pulse Duration $\tau_{\text{pulse}} = 1/\Delta\nu$	Observed Pulse Duration
Ti^{3+}:Al_2O_3	H	100 THz	10 fs	10 fs
Rhodamine-6G dye	H/I	40 THz	25 fs	27 fs
Nd^{3+}:Glass (phosphate)	I	7 THz	140 fs	150 fs
Er^{3+}:Silica fiber	H/I	5 THz	200 fs	200 fs
Nd^{3+}:YAG	H	150 GHz	7 ps	7 ps
Ar^+	I	3.5 GHz	286 ps	150 ps
He–Ne	I	1.5 GHz	667 ps	600 ps
CO_2	I	60 MHz	16 ns	20 ns

[a]The transition linewidths $\Delta\nu$ are drawn from Table 14.3-1.

EXAMPLE 15.4-2. ***Mode-Locking in an Ytterbium-Doped Fiber Laser.*** A passively mode-locked ytterbium-doped silica fiber laser operated at $\lambda_o = 1070$ nm produces an average power of 10 W in the form of pulses with energy 200 nJ and peak power 40 kW. This laser generates mode-locked pulses that are 5 ps in duration at a repetition rate of 50 MHz. Since $\Delta\nu = 5$ THz, the pulse duration is substantially greater than the expected value, $\tau_{\text{pulse}} = 1/\Delta\nu = 200$ fs. The discrepancy arises because of group velocity dispersion, which imparts broadening and chirping to a pulse traveling through an optical medium (see Fig. 5.6-3). The normal dispersion in a silica fiber near $\lambda_o = 1$ μm (Fig. 5.6-5) can be canceled by introducing anomalous dispersion via a fiber Bragg grating or a photonic-crystal fiber, reducing the observed pulse duration to 200 fs.

How to make the modes lock together

A active switching: acoustics optics and electro-optics switching

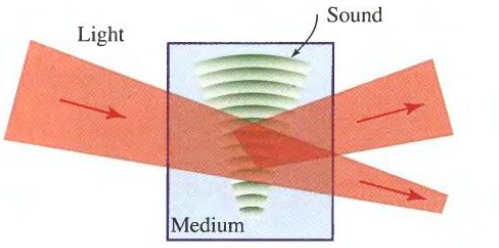

Compressing ->
refractive index difference

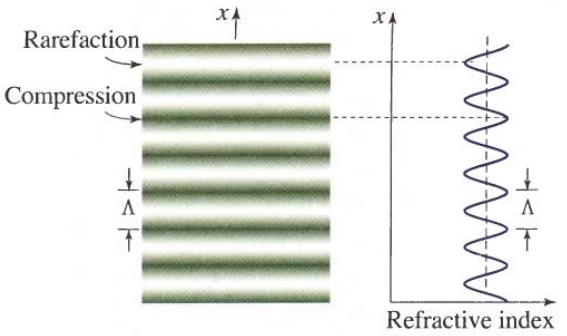

Figure 19.0-1 Sound modifies the effect of an optical medium on light.

$$\sin\theta = \frac{\lambda}{2\Lambda},$$

Bragg diffraction,

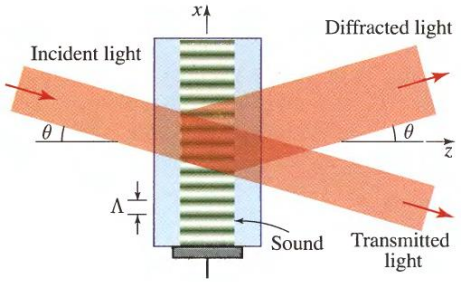

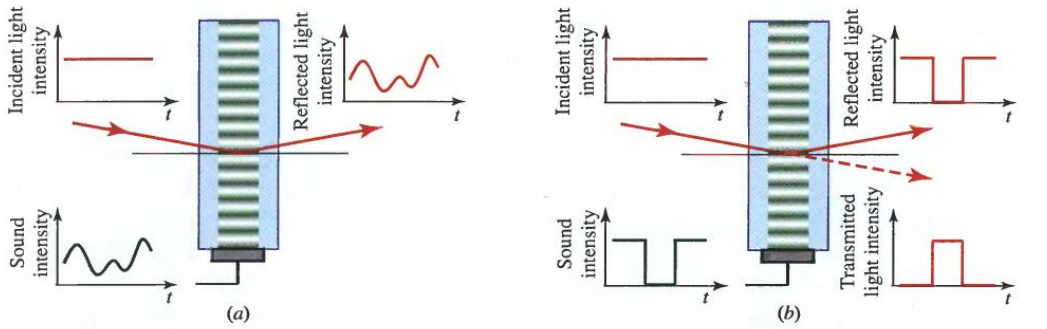

Figure 19.2-1 (*a*) An acousto-optic modulator. The intensity of the reflected light is proportional to the intensity of sound. (*b*) An acousto-optic switch.

How to make the modes lock together

Electro-optics switching

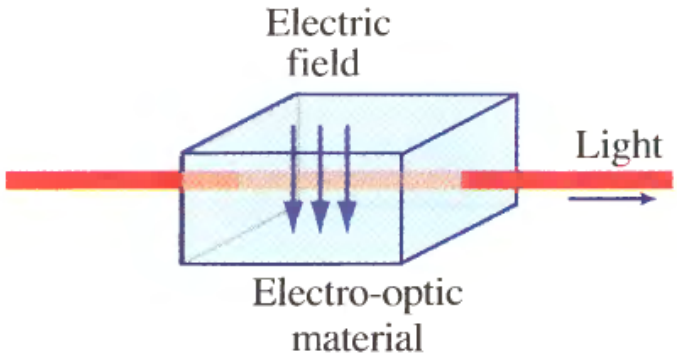

Figure 20.0-1 A steady electric field applied to an electro-optic material changes its refractive index. This in turn changes the effect of the material on light traveling through it. The electric field therefore controls the light.

A. Pockels and Kerr Effects

$$n(E) = n + a_1 E + \tfrac{1}{2} a_2 E^2 + \cdots,$$

where the coefficients of expansion are $n = n(0)$, $a_1 = (dn/dE)|_{E=0}$, and $a_2 = (d^2n/dE^2)|_{E=0}$. For reasons that will become apparent below, it is conventional to write (20.1-1) in terms of two new coefficients, $\mathfrak{r} = -2a_1/n^3$ and $\mathfrak{s} = -a_2/n^3$, known as the electro-optic coefficients, so that

$$n(E) = n - \tfrac{1}{2}\mathfrak{r}\, n^3 E - \tfrac{1}{2}\mathfrak{s}\, n^3 E^2 + \cdots. \qquad (20.1\text{-}2)$$

Pockels Effect

$$n(E) \approx n - \tfrac{1}{2}\mathfrak{r}\, n^3 E,$$

Kerr Effect

$$n(E) \approx n - \tfrac{1}{2}\mathfrak{s}\, n^3 E^2.$$

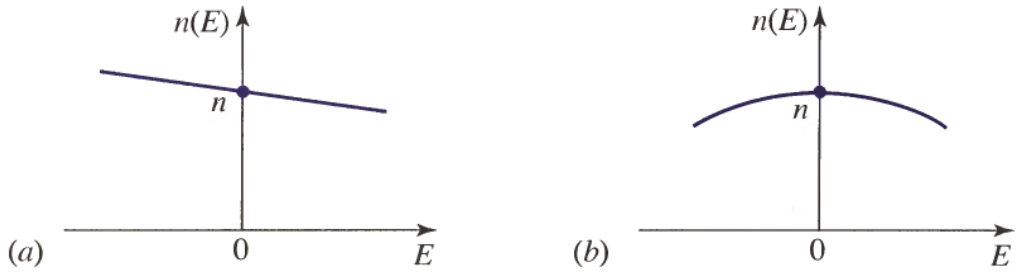

Figure 20.1-1 Dependence of the refractive index on the electric field: (*a*) Pockels medium; (*b*) Kerr medium.

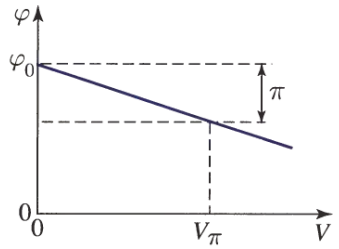

$$\varphi = \varphi_0 - \pi \frac{V}{V_\pi},$$

(20.1-7)
Phase Modulation

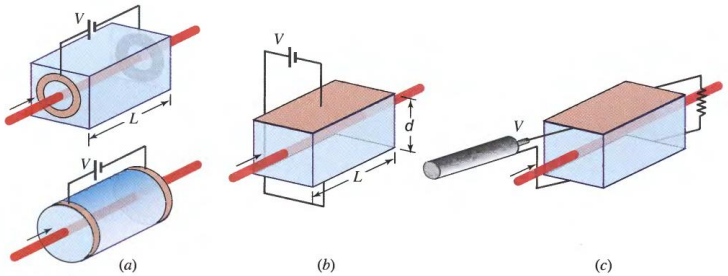

Figure 20.1-2 (*a*) Longitudinal modulator. The electrodes may take the shape of washers or bands, or may be transparent conductors. (*b*) Transverse modulator. (*c*) Traveling-wave transverse modulator.

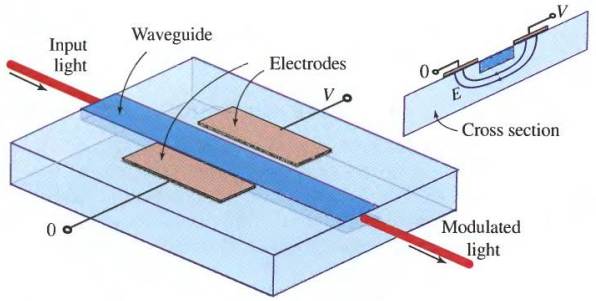

Figure 20.1-3 An integrated-optical phase modulator using the electro-optic effect.

How to make the modes lock together

A passive switching: Saturable absorber

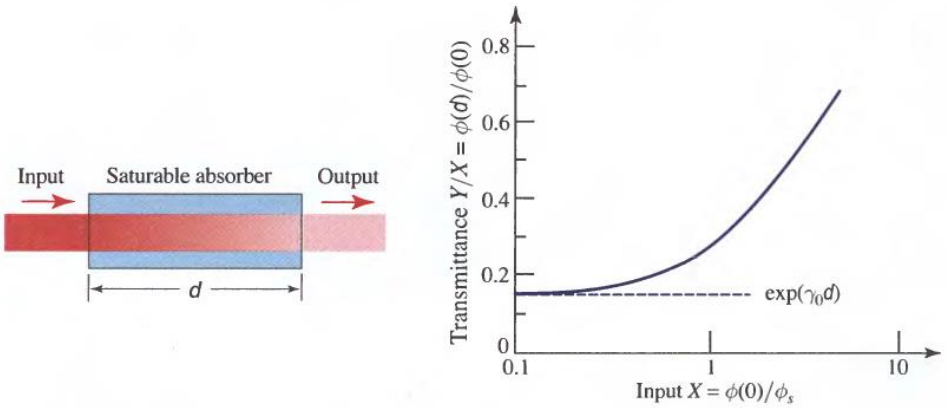

Figure 14.4-4 The transmittance of a saturable absorber $Y/X = \phi(d)/\phi(0)$ versus the normalized photon-flux density $X = \phi(0)/\phi_s$, for $\gamma_0 d = -2$. The transmittance increases with increasing input photon-flux density.